Epitaxial Growth of Highly Compressively Strained Gesn Alloys Up To 12.5% Sn

Jurabek Abdiyev[1], Sadulla Saydullayev[1], Elyor G'aybulloyev[2], Sherzod Yarashev[2*], Bekzod Erkinov[2]

[1]Physical-technical Institute of NPO "Physics – Sun" of Uzbekistan Academy of Sciences Uzbekistan, Tashkent, Chingiz Aitmatov street 2B.
[2]Tashkent University of Information Technologies named after Muhammad al-Khwarizmi, Uzbekistan, Tashkent, Amir Temur street 108.
Corresponding author: sherzodyarashev1997@gmail.com (Sh. Yarashev)

Abstract: This paper reports on the growth and characterization of highly compressive strained GeSn layers on thin strain relaxed Ge virtual substrates on Si wafers. Sn concentration up to 12.5%, which is about more than 10 times the thermal equilibrium predicted for GeSn binaries, are successfully epitaxially grown by ultra-low temperature (160 1C) molecular beam epitaxy. A minimum channeling yield of 9% evidence the high crystalline quality of the GeSn alloys while angular channeling scan demonstrate that all GeSn layers are fully pseudomorphic on the relaxed Ge virtual substrate. The strain analysis shows a deviation from the Vegard's law for Sn contents above 8%. The analysis is completed by the Raman mode dependence on the alloys composition.

Keywords: A3. Molecular beam epitaxy, B3. Heterojunction semiconductor devices.

1. INTRODUCTION.

The indirect band-gap materials based on group IV elements C, Si and Ge and their alloys constitute the base of today's IC industry: Si is like the heart of the high performance or low power micro-electronics, while Si:C and SiGe are used in source and drain regions of transistors as stressors. However, the use of indirect semiconductors in optical applications is relatively restricted because the performance of their optical devices is limited [1–3]. The introduction of strain, also called strain engineering, allows the modification of essential material properties, like carrier mobility [4], effective mass or band-gap, dopant solubility [5], [6] which in turn increase their applicability. Ge, an excellent channel material in CMOS applications [7], undergoes the most interesting metamorphosis: under a biaxial strain of about 2% it becomes a direct band-gap semiconductor [8]. Recently, a tensile strain of 1.3% was reported for Ge layers epitaxially grown on partial relaxed $Ge_{0.9}Sn_{0.1}$ buffers [9]. Moreover, for this buffer theoretical calculations predict indirect to direct transition as well as for tensile strained GeSn alloys with 6.3% Sn [11]. This strain-induced transformation opens new ways for improving nano- and optoelectronic devices as recently proposed for energy efficient tunnel field effect transistors [9], [11].

In the recent years, huge progress has been achieved in the development of epitaxial growth techniques which gave an enormous boost to the epitaxial growth of Ge on Si and GeSn on Si or Ge. Besides the deposition of GeSn through MBE [12], [13], the deposition through CVD (chemical vapor deposition) has been recently reported through the development of new precursors like Ge_2H_6, SnD_4 [14–16]. Another promising method to incorporate Sn into the SiGe and Ge matrixes is pulsed laser induced epitaxy [17], [18]. Three major obstacles have to be overcome in the epitaxial growth of GeSn alloys: the large lattice mismatch between Ge and α-Sn of 14.7%, the low solubility of Sn in the Ge matrix of about 1% [19] and the Sn surface segregation at growth temperatures higher than 140 1C [20]. An ultra-low tempera-ture molecular beam epitaxy (MBE) growth process may be employed to avoid the above shortcomings [21].

Despite that the breakthrough in active photonics components like LED or lasers is expected to appear with the demonstration of a direct band-gap in Ge and GeSn, other optical components like integrated GeSn detectors [22–24] and emitters [25–27] were demonstrated on compressively strained GeSn alloys.

In this paper we present the epitaxial growth of GeSn alloys with a substitutional Sn content up to 12.5%. Using precise angular channeling scans and Raman spectroscopy we demonstrate that the grown layers are pseudomorphic on Ge VS and are of high single-crystal quality.

2. EXPERIMENTAL PROCEDURE.

The growth experiments were performed in a solid-source MBE equipment for 150 mm substrates, schematically presented in Fig. 1 [28]. The system works under ultra-high vacuum conditions with a base pressure below 10^{10} mbar. The most critical growth parameter is the substrate temperature, which influences all adatom surface processes, the crystalline growth and the surface morphology. The substrate is heated by a graphite meander through radiant heating. The real surface temperature and the dynamic cooling processes were calibrated by thermo-couples integrated on a specially designed Si substrate because at growth temperatures below 600 1C the heater radiative emission spectrum and the Si absorption spectrum exhibit only a small overlap.
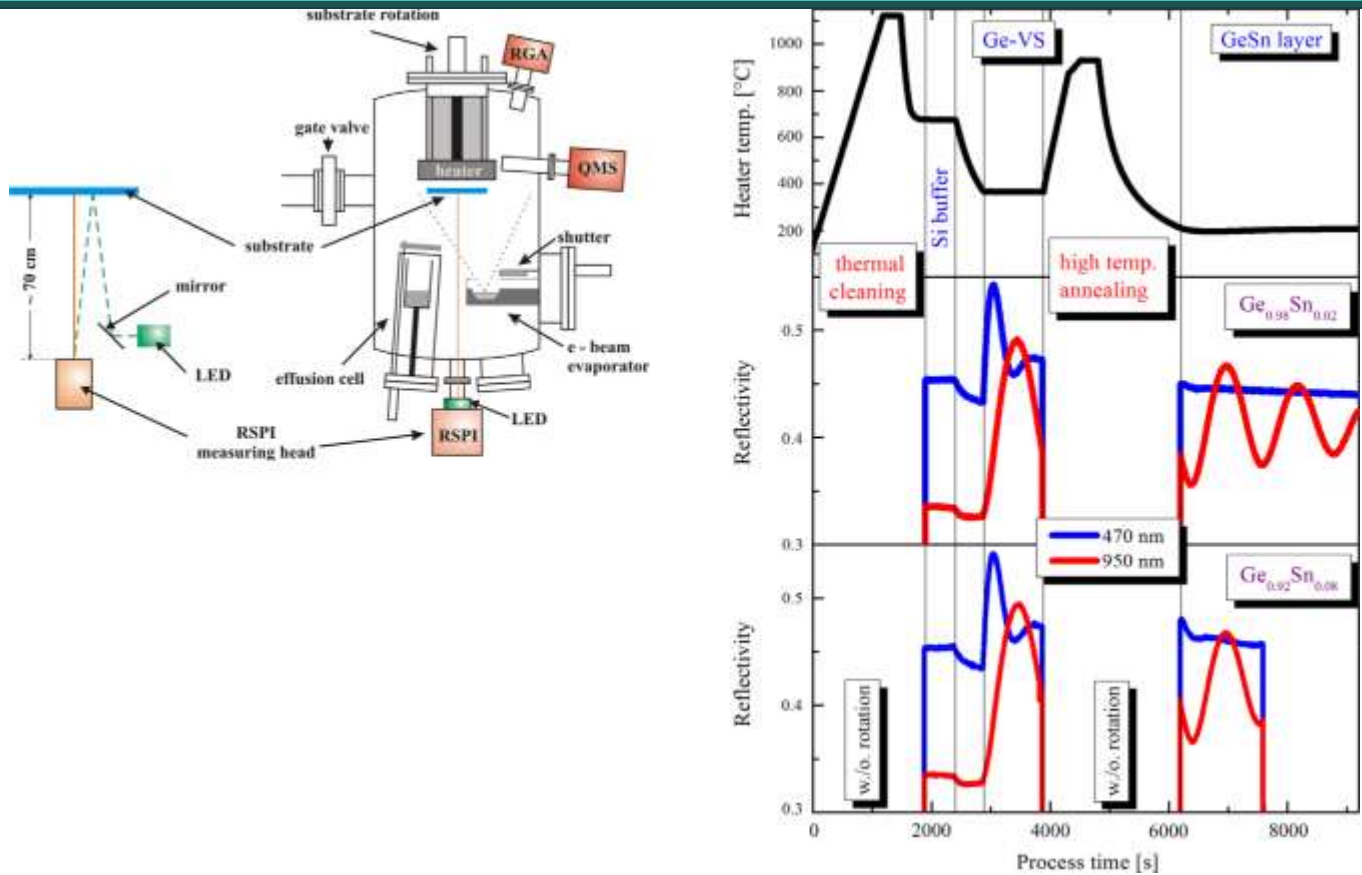
Fig. 1. Schematic illustration of a group IV MBE growth chamber with an in-situ reflection supported pyrometric interferometry system.

At 400 1C the maximum thermal radiation of a black emitter has a wavelength of 4.3 mm where the intrinsic Si is transparent. The heating of the substrate at low temperatures is caused mainly by free carrier absorption.

For the deposition of Si, an electron beam evaporator (EBE) was used, to avoid the contact of the extreme reactivity molten Si with the crucible. The matrix material Ge is evaporated from a special effusion cell with a pyrolithic BN crucible [29]. An advantage of the effusion cell over the EBE is the extremely low flux fluctuation at high Ge rate. The absolute calibration of the Ge flux was based on spectroscopic ellipsometry measurements of Ge layer thickness on Si substrates. The very low melting point of Sn of 232 1C requires the use of a special Sn effusion cell with a dual filament in order to suppress the creep characteristics of the liquid Sn. Crucible temperatures between 1000 1C and 1120 1C are applied to achieve Sn concentrations between 0% and 12.5%. The absolute calibration of the Sn effusion cell was made ex-situ by Rutherford Back-scattering Spectroscopy (RBS).

The growth parameters are monitored by different in-situ methods, such as flux measurement, residual gas composition but we emphasis here a reflection supported pyrometric interferometry system (RSPI) [30]. The RSPI consists of a pyrometer and reflectometer working at two optical wavelengths of $\lambda \frac{1}{4} 470$ nm and $\lambda \frac{1}{4} 950$ nm (see Fig. 1). The reflectometer signal at $\lambda \frac{1}{4} 950$ nm is used for real-time determination of the emissivity, thus allowing the determination of temperatures even for arbitrary multi-layer stacks. The reflectivity measurements permit the monitoring of the crystalline growth even at very low temperatures. Note that the layer stack thicknesses must be chosen to prevent an undesired breakdown of crystalline growth [31].

100 mm Si (Czochralsky type) with a specific resistance of 10–20 Ω cm (p-type) were used. An in-situ thermal cleaning step at 900 1C was performed in order to remove the natural surface SiO_2 [32]. An example of an GeSn epitaxial growth on Ge VS on Si substrate is presented in Fig. 2. The upper image shows the heater temperature while, the middle and the bottom plots show the reflectometer signals, at both $\lambda \frac{1}{4} 470$ nm and $\lambda \frac{1}{4} 950$ nm wavelengths, as a function of the process time for growth of GeSn alloys with 2% and 8% Sn content, respectively.

The epitaxial growth starts with a 50 nm Si buffer grown at 600 1C, to reconstruct the ideal Si crystal, followed by a tempera-ture decrease to 330 1C for the Ge VS growth and a subsequent high temperature annealing step at 810 1C for dislocation reduction. At these high temperatures Si atoms diffuse into the Ge layer generating a thin SiGe interface layer.

Fig. 2. Overview of the complete epitaxial process for growth of GeSn layers on a Si substrate with a Ge VS. Top: heater temperature as function of process time. Middle: reflectivity under vertical incidence vs. process time at two wavelengths $\frac{1}{4} 470$ nm and $\lambda \frac{1}{4} 950$ nm for a GeSn film with 2% Sn content. Bottom: Reflectivity vs. process time for a GeSn film with 8% Sn content.

During the heating/cooling process an in-plane tensile strain may be incorporated into the Ge VS due to thermal mismatch of Si and Ge. However, the annealing/ cooling parameters and the thickness of the Ge layer were chosen so that the Ge VS presents the same lattice constant as Ge bulk. Finally the temperature was decreased to 160 1C and the GeSn layers with different Sn concentrations between 0% and 12.5% were deposited. In order to avoid strain relaxation or epitaxial breakdown the layer thickness was reduced with the increase of Sn content.

A typical in-situ reflection measurement during the growth process of a $Ge_{0.98}Sn_{0.02}$ layer is shown in the middle graph in Fig. 2. During the growth of the Si buffer the reflection of both wavelengths are constant. Typical thickness interferences can be observed during the growth of the Ge VS. After the high tempera-ture annealing step the GeSn layer is grown. The reflectivity at ¼950 nm shows here also the typical thickness interferences (see Fig. 2). Due to the small penetration depth in Ge at λ¼4470 nm of about 17 nm [33], the oscillation of the reflectivity of the GeSn layer cannot longer be observed. A small decrease of the reflection signal is measured, attributed to a slight increase of the surface roughness. The bottom graph in Fig. 2 shows the in-situ reflection measurement of the epitaxial growth of a GeSn layer with 8% Sn. The curves show a similar behavior as presented above. The growth time for the 12.5% Sn sample is relatively short (about 340 s) which does not permit observation of a complete oscillation cycle.

The absolute Sn concentration, the layer quality and the strain statue of different GeSn layers were analyzed by RBS. The lattice vibration modes were studied by Raman spectroscopy. The results of RBS and Raman are later compared.

3. RESULTS AND DISCUSSION.

Using the growth process described above, we have grown thin Ge VS followed by the growth of GeSn layers. The crystalline quality of the GeSn layers is investigated by Rutherford Back-scattering Spectroscopy/Channeling (RBS/C) using a Tandetron accelerator with 1.4 MeV He[b] ions. The RBS technique is also employed to determine with an accuracy of 0.5% the layer stoichiometry and the thickness of the GeSn layers.

Fig. 3 presents the RBS/C spectra of a 115 nm $Ge_{0.92}Sn_{0.08}$ (sample F) on 85 nm Ge VS (Fig. 3 (a)) and a 34 nm $Ge_{0.875}Sn_{0.125}$ layer (sample G) grown on a 80 nm Ge VS (Fig. 3 (b)). No de-channeling is observed towards the GeSn/Ge interface (low energy edge of the Sn signal) indicating pseudomorphic GeSn growth on Ge VS. The minimum channeling yield, defined as the ratio of the intensity of the random and channeling spectra taken below the surface peak signal, amounts to 9% for the GeSn layer, identical with the minimum yield of the Ge-VS. The extracted layer thicknesses for all investigated GeSn samples are listed in Table 1.

A powerful method for analyzing strain states in layer systems is the measurement of changes in the ion channeling directions. Recently, a systematic derivation and compilation of the required relations between the strain induced angle changes and the components of the strain tensor for general crystalline layer systems of reduced symmetry compared to the basic cubic crystal was published [34]. In the past, planar {100} and {110}SiGe/Si layer systems as well as nano-patterned structures layers characterized by plane stress and tetragonal strain states have been analyzed by RBS/C using a high-precision goniometer [35–37].

For GeSn (001) samples, we have chosen angular scans along a plane through the [001] sample normal and the inclined [11] direction. In a cubic crystal, the angle between the [001] sample normal and an inclined [011] direction amounts to 451. If the crystalline layer is under biaxial compression in the growth plane, due to its larger lattice constant compared to the underlying substrate, the lattice constant perpendicular to the growth plane will increase according to the Poisson effect. As a result the angle between both directions is shifted by an amount of θ to an angle smaller than 451. Fig. 4 shows channeling angular yield scans of the Sn backscattering signal for samples C to G presented in Table 2. The scans through the [001] sample normal as well as the scan through the inclined [011] crystal axis of a cubic crystal structure are shown for reference. The position of the scan minimum represents the absolute angle θ between the [001] sample normal and the inclined [011] direction. The angular shift is related to the amount of tetragonal strain defined as which describes the tetragonal strain ε_T as a function of the angular displacement θ, the degree of strain relaxation can be determined [38]. In Table 2 the values of angular displacement for GeSn layers with different Sn content and the corresponding tetragonal strain are given. The measured angle changes are in rough (within 25%) agreement with the theoretical angle changes calculated using the Vegard's law up to a Sn content of 8%. Above this concentration, the measurements indicate a larger elastic strain in the GeSn layer as theoretically possible for pseudo-morphic growth. This apparent inconsistency is a clear indication that the Vegard's law is no more accurate for higher Sn content

Fig. 3. RBS/C spectra of 115 nm $Ge_{0.92}Sn_{0.08}$ on 85 nm Ge VS (a) and of a 34 nm $Ge_{0.875}Sn_{0.125}$ layer grown on a 80 nm Ge VS. (b) A minimum channeling yield of 9% evidence high crystalline quality.
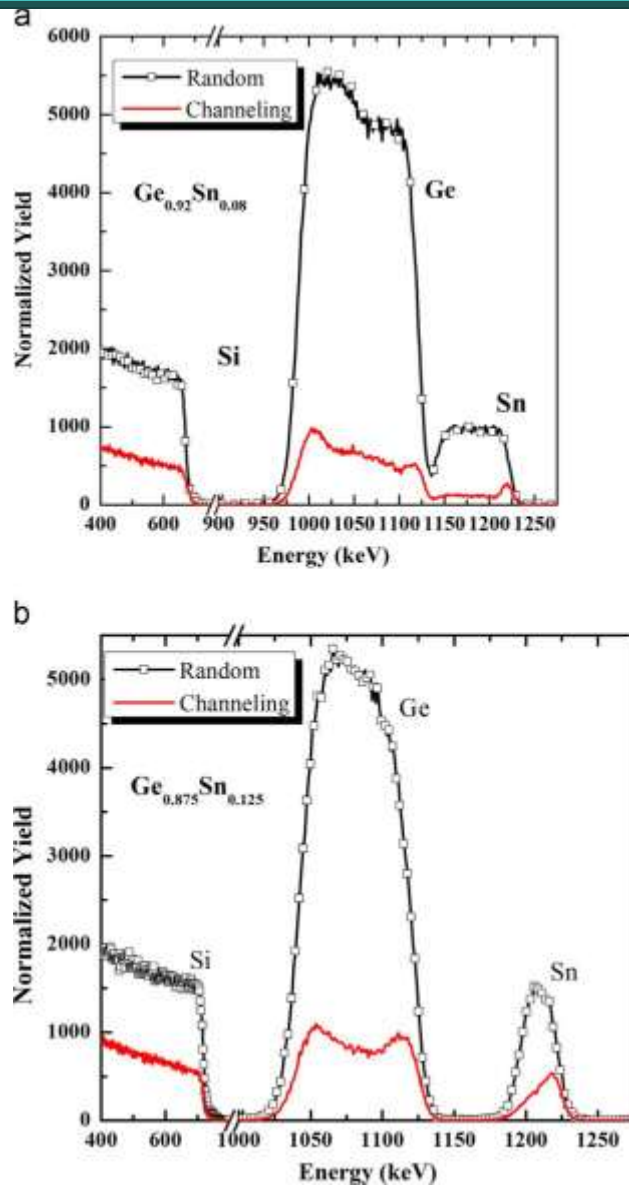
Table 1
Overview of RBS results of the investigated GeSn samples.

Sample	RBS analysis	
	Sn content [%]	Thickness GeSn [nm]
A	0	–
B	2.4	261
C	4.7	255
D	6	255
E	8	115
F	11	45
G	12.5	34

layers. The angular channeling scans prove that all our investigated layers are pseudomorphically grown compressively strained on the relaxed Ge VS. The extremely high tetrahedral strain of up to 3.2% is possible because of metastable growth at the very low temperature of 160 1C.

The m-Raman measurements were carried out at room temperature in the backscattering arrangement with an in Via Raman microscope system. This system is equipped with a CCD camera and a Leica microscope. A grating with 1800 lines/mm was used for all measurements.
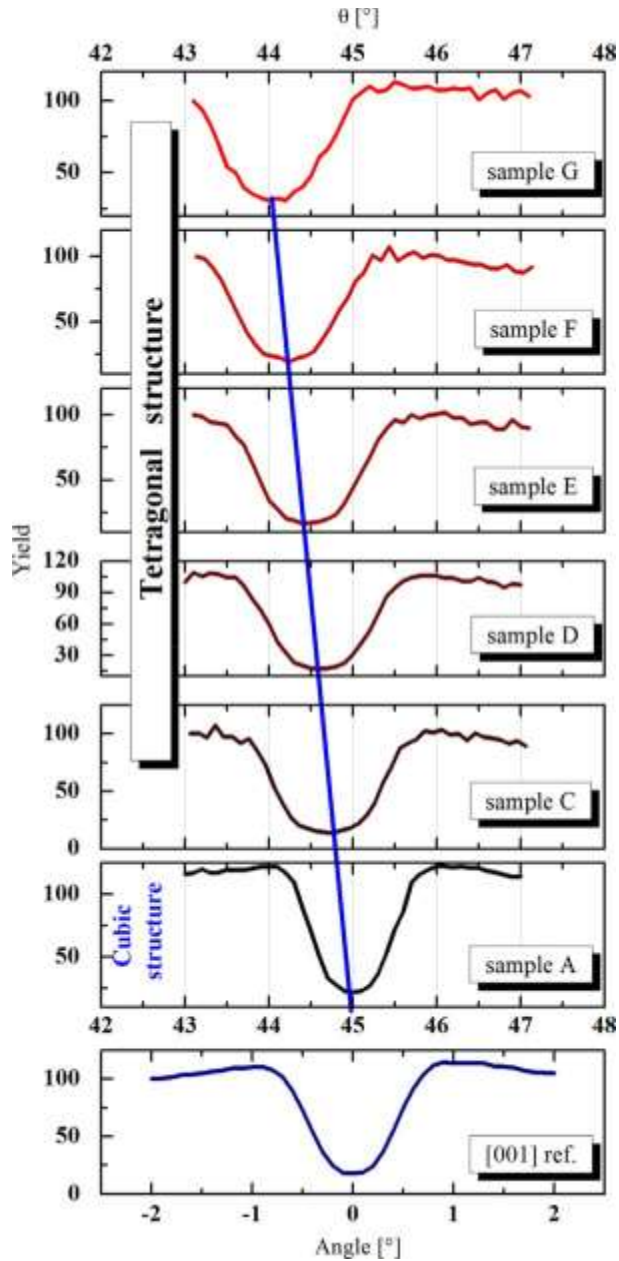

Fig. 4. Channeling angular yield scans for the determination of tetragonal strain of GeSn samples presented in Table 2. The scans through the [100] sample normal as well as the scan through the inclined [110] crystal axis (sample A) of a cubic crystal structure are shown for reference. The curves of sample C to sample G show the corresponding yield of the Sn signal. Increasing shift of the minimum with respect to 451 indicates an increasing amount of tetragonal strain in the GeSn crystal lattice.

A helium–neon laser with a wavelength of 633 nm and a power of 10 mW was used as excitation source. The Raman spectra were carried out in a static mode with an exposure time of 1 s and a total of 20 accumulations, in order to prevent the heating of the sample by the laser. The laser spot was focused with a 50 objective on to the surface. The spectra were fitted with a mixture of Gaussian and Lorentzian to obtain the best possible results in terms of peak position, intensity and line width. A detailed description of this fitting program is found in Ref. [39]. The Raman system resolution is 70.2 cm[1] due to the grid used.

The room temperature Raman spectra of strained GeSn samples with different Sn concentrations (data from RBS measurements — see Table 1) are presented in Fig. 5. The spectrum of the Ge reference sample (Sample A) is also added. The intensity of the Ge–Ge peak at 300 cm[1] decreases continuously with increasing the Sn content and shifts to lower wavenumbers. Besides the main peak, the spectra shows further distinct mode contributions: In the range between 250 cm[1] and 300 cm[1], the spectra show

complementary to the Ge reference the typical GeSn peak at 262 cm [1] and, furthermore, a second peak at 285 cm [1] that causes a shoulder in the rising edge of the Ge–Ge peak. At the lower wavenumber of 185 cm [1] a further peak is observed, attributed by D'Costa et al. to a Sn–Sn like mode frequency [40]. For the investigated GeSn alloys this vibration mode shifts stronger (10 cm [1]) with the Sn content compared to the other Raman modes. The 2TA Ge–Ge peaks at 160 cm [1] complete the Raman spectra.

For analysis of the Ge–Ge and Ge–Sn peaks the background of the Raman system was subtracted before the spectra fitting and the simulation results are plotted in Fig. 6 as the difference of the Raman shift between the Ge reference and GeSn layers versus the Sn content. For fully strained GeSn layers on Ge (100) the theoretical description for the change in the Ge–Ge Raman shift where x is the Sn content. Our experimental data agrees with the theoretical prediction up to a content of 6% Sn as well as with the measurement data of Su et al. [41]. For higher Sn concentrations significant deviations from the linear behavior are observed. Also the sample with 8% Sn exhibits a smaller change (0.5 cm [1]) in the Raman shift compared with the experimental data in Ref. [23]. The samples with high Sn concentrations have reduced layer thicknesses because the lower critical layer thickness for pseudomorphic growth.

The penetration depth of the excitation laser light at $\lambda \frac{1}{4} 633$ nm is about 62 nm in Ge [33] and 30 nm in relaxed $Ge_{0.85}Sn_{0.15}$ [42]. The thickness of the GeSn layer with a Sn content of 12.5% is 37 nm, larger as the penetration depth resulting in superposition of the Ge–Ge vibration modes of the GeSn and Ge VS. However, this superposition does not occur for the case of the Ge–Sn peak at 262 cm [1]. The relative intensity change, I, of the Ge–Ge mode of the GeSn layers with respect to the reference intensity I_0 of the Ge layer as function of the Sn content is shown in the inset of Fig. 6. There is a linear decrease in the intensity observed with increasing the Sn content. The Raman intensity of the Ge–Ge peak decreases to about 25% in a GeSn alloy with a Sn concentration of 12.5%.

Table 2

Values of angular displacement for GeSn layers with different Sn contents and the corresponding tetragonal strain.

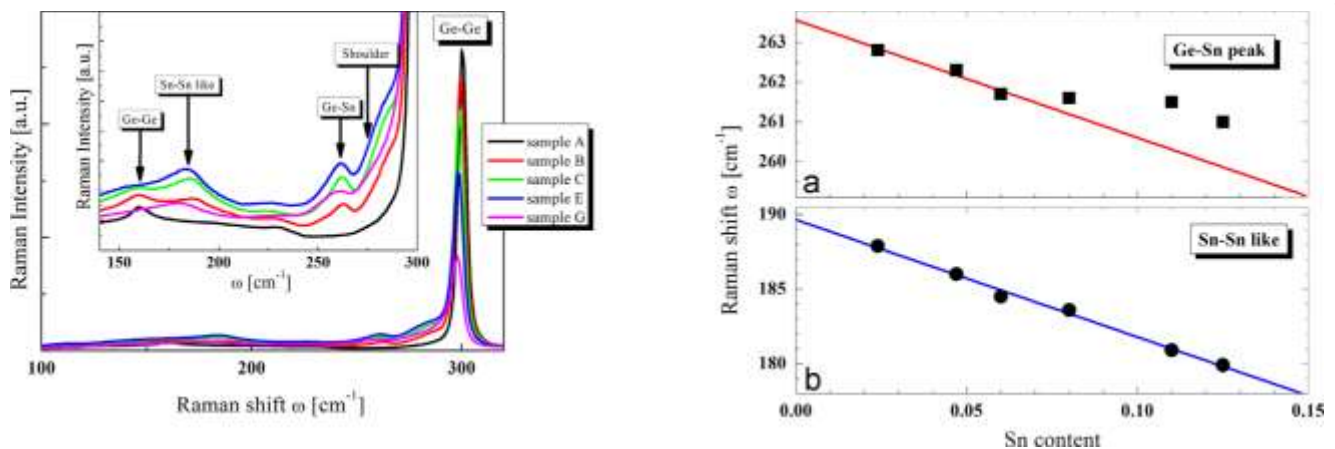| Sample	Sn content RBS	a_o [nm] (Vegard's law)	f [%] lattice mismatch with Ge	Θ_{theo} [deg] pseudomorph	Tetragonal strain Θ_{exp} [deg][%]
C	0.047	0.56966	0.69	0.34	0.301.0
D	0.06	0.57074	0.88	0.44	0.391.4
E	0.08	0.5724	1.18	0.58	0.531.9
F	0.11	0.5749	1.62	0.80	0.772.7
G	0.125	0.57614	1.84	0.91	0.933.2

75

Fig. 5. Raman spectra of GeSn samples with different Sn concentrations. Besides the main peak of the Ge–Ge mode at 300 cm [1] further Raman modes can be observed. The inset shows an enlarged view of it. The Ge–Sn peak at 262 cm [1], a distinct shoulder in the range of 285 cm [1], a peak at 185 cm [1] and the 2TA Ge–Ge peak at 160 cm [1].
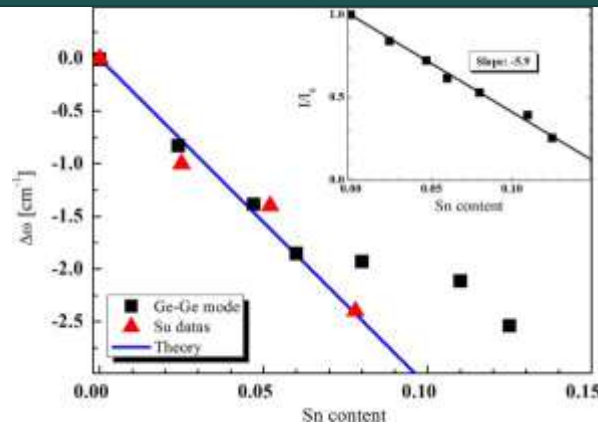
Fig. 7. Compositional dependence of the Ge−Sn mode frequency (a) and the Sn−Sn like mode (b) in GeSn alloys. The Ge−Sn peak position shows linear dependence with Sn content up to 6% Sn. At higher concentration, a deviation from the linear course is observed. In contrast to this, the "Sn−Sn like" mode frequency shows a linear relationship with Sn concentration over the complete investigated alloy composition.

Fig. 6. Difference of Raman shift of Ge−Ge signals of GeSn and Ge VS as function of Sn concentration. For comparison, the theoretically expected characteristic and the measurement data of Su et al. [41] are added. Inset: relative change of the intensity with respect to the Ge reference vs. Sn content.

The Raman shift of the Ge−Sn mode as a function of Sn concentration is shown in Fig. 7(a). The Raman shift ω_{Ge-Sn} with Sn contents up to 6% can be linearly calculated with For Sn concentrations greater than 6% the same deviation as for the Ge−Ge mode is observed. The Ge-VS is, therefore, not respon-sible for the deviation from the theoretically predicted linear trend while Ge shows in this wavelength range only the background signal. The "Sn−Sn like" peak was observed for all GeSn layers. The Raman shift ω_{Sn-Sn} as a function of the Sn content is shown in Fig. 7(b). In contrast to the other two observed Raman peaks a linear relationship was found:

The Sn−Sn mode of the α-Sn is present at the wavenumber of 197 cm[1] [43]. However, this vibration mode is hard to be observed for low Sn concentrations, because the number of Sn−Sn neighbors is statistically very low and consequently, the signal of the Sn−Sn mode is too weak to be detected [44]. From our observations we cannot affirm that we see a Sn−Sn peak, in agreement with Ref. [40] – and we use the term "Sn−Sn like".

4. CONCLUSION.

In this paper we have presented the epitaxial growth of highly compressive strained GeSn layers with a Sn concentration up to 12.5% on thin Ge-VS on Si substrates. The GeSn layers were grown by ultra-low MBE on strain relaxed Ge-VS. A minimum RBS channeling yield of 9% proves the high quality of the grown GeSn crystals comparable with that of the underlying Ge VS and, very important, that more than 90% of the Sn atoms occupy lattice positions. Precise angular channeling scan was performed to determine the strain status of these layers. All layer proved to be pseudomorph with the maximum tetragonal strain value of 3.2% for the GeSn layer with 12.5% Sn content. Using strain measurements a slight deviation from the Vegard's law for Sn contents above 8% is observed.

Knowing the strain status of our layer we had a look into the Raman modes dependence on the alloy concentration. The Ge−Ge peak position and the Ge−Sn peak position shows linear depen-dence with Sn content up to 6% Sn. At higher concentrations, a deviation from the theoretical course was found. Another Raman mode was determined in the range between 190 cm[1] and 180 cm[1]. This mode frequency shows a linear relationship with Sn concentrations over the complete investigated alloy composi-tion. In contrast to the other two Raman modes, which show a much weaker change of Raman shifts, this mode shifts up to 10 wave numbers with a Sn content of 12.5%.

REFERENCES

[1] M. Oehme, J. Werner, E. Kasper, M. Jutzi, M. Berroth, Applied Physics Letters 89 (2006) 071117.
[2] D. Buca, S. Winnerl, S. Lenk, C. Buchal, D.X. Xu, Applied Physics Letters 80 (2002) 4172.
[3] D. Buca, S. Winnerl, S. Lenk, S. Mantl, Ch. Buchal, Journal of Applied Physics 92 (2002) 7599.
[4] S.F. Feste, Th. Schäpers, D. Buca, Q.T. Zhao, J. Knoch, M. Bouhassoune, Arno Schindlmayr, S. Mantl, Applied Physics Letters 95 (2009) 182101.
[5] F. Lanzerath, D. Buca, H. Trinkaus, M. Goryll, S. Mantl, J. Knoch, U. Breuer, W. Skorupa, B. Ghyselen, Journal of Applied Physics 104 (2008) 044908.

[6] W. Heiermann, D. Buca, H. Trinkaus, B. Hollaender, U. Breuer, N. Kernevez,
B.   Ghyselen, S. Mantl, ECS Transactions 19 (2009) 95.
[7] B. Vincent, Y. Shimura, S. Takeuchi, T. Nishimura, G. Eneman, A. Firrincieli,
J. Demeulemeester, A. Vantomme, T. Clarysse, O. Nakatsuka, S. Zaima,
J.   Dekoster, M. Caymax, R. Loo, Microelectronic Engineering 88 (2011) 342.
[8] M. El Kourdi, G. Fishman, S. Saauvage, P. Boucaud, Journal of Applied Physics 107 (2010) 013710.
[9] S. Wirths, A.T. Tiedemann, Z. Ikonic, P. Harrison, B. Holländer, T. Stoica,
G.   Mussler, M. Myronov, D. Buca, S. Mantl, Applied Physics Letters 102 (2013) 192103.
[11] R. Kotlyar, U.E. Avci, S. Cea, R. Rios, T.D. Linton, K.J. Kuhn, I.A. Young, Applied Physics Letters 102 (2013) 113106.
[12] S. Takeuchi, A. Sakai, K. Yamamoto, O. Nakatsuka, M. Ogawa, S. Zaima, Semiconductor Science and Technology 22 (2007) 231.
[13] J. Werner, M. Oehme, M. Schmid, M. Kaschel, A. Schirmer, E. Kasper, J. Schulze, Applied Physics Letters 98 (2011) 061108.
[14] J. Kouvetakis, A.V.G. Chizmeshya, Journal of Materials Chemistry 17 2007 1649.
[15] F. Gencarelli, B. Vincent, L. Souriau, O. Richard, W. Vandervorst, R. Loo,
M.   Caymax, M. Heyns, Thin Solid Films 520 (2012) 3211.
[16] S. Wirths, D. Buca, G. Mussler, a.T. Tiedemann, B. Hollander, P. Bernardy,
T.   Stoica, D. Grutzmacher, S. Mantl, ECS Journal of Solid State Science and Technology 2 (2013) N99.
[17] S. Stefanov, J.C. Conde, A. Benedetti, C. Serra, J. Werner, M. Oehme, J. Schulze,
D.   Buca, B. Holländer, S. Mantl, S. Chiussi, Applied Physics Letters 100 (2012) 104101.
[18] S. Stefanov, J.C. Conde, A. Benedetti, C. Serra, J. Werner, M. Oehme, J. Schulze,
D.   Buca, B. Holländer, S. Mantl, S. Chiussi, Applied Physics Letters 100 (2012) 204102.
[19] C.D. Thurmond, F.A. Trumbore, M. Kowalchik, Journal of Chemical Physics 24 (1956) 799.
[20] P.R. Pukite, A. Harwit, S.S. Iyer, Applied Physics Letters 54 (1989) 2142.
[21] E. Kasper, J. Werner, M. Oehme, S. Escoubas, N. Burle, J. Schulze, Thin Solid Films 520 (2012) 3195.
[22] R. Roucka, J. Mathews, C. Weng, R. Beeler, J. Tolle, J. Menéndez, J. Kouvetakis, IEEE Journal of Quantum Electronics 47 (2011) 213.
[23] S. Su, B. Cheng, C. Xue, W. Wang, Q. Cao, H. Xue, W. Hu, G. Zhang, Y. Zuo,
Q.   Wang, Optics Express 19 (2011) 6400.
[24] M. Oehme, M. Schmid, M. Kaschel, M. Gollhofer, D. Widmann, E. Kasper,
J.   Schulze, Applied Physics Letters 101 (2012) 141110.
[25] M. Oehme, J. Werner, M. Gollhofer, M. Schmid, M. Kaschel, E. Kasper,
J.   Schulze, IEEE Photonics Technology Letters 23 (2011) 1751.
[26] R. Roucka, J. Mathews, R.T. Beeler, J. Tolle, J. Kouvetakis, J. Menéndez, Applied Physics Letters 98 (2011) 061109.
[27] M. Oehme, E. Kasper J. Schulze, ECS Journal of Solid State Science and Technology 2 (2013) R76.
[28] M. Oehme, J. Werner, M. Kaschel, O. Kirfel, E. Kasper, Thin Solid Films 517 (2008) 137.
[29] M. Oehme, M. Bauer, E. Kasper, Materials Science and Engineering B89 (2002) 332.
[30] M. Bauer, M. Oehme, M. Sauter, G. Eifler, E. Kasper, Thin Solid Films 364 (2000) 228.
[31] M. Bauer, M. Oehme, E. Kasper, Materials Science and Engineering B89 (2002) 263.
[32] E. Kasper, M. Bauer, M. Oehme, Thin Solid Films 321 (1998) 148.
[33] R.F. Potter, Handbook of Optical Constants of Solids II Academic, New York (1985) 465.
[34] H. Trinkaus, D. Buca, B. Holländer, R.A. Minamisawa, S. Mantl, J.M. Hartmann, Journal of Applied Physics 107 (2010) 124906.
[35] B. Holländer, H. Heer, M. Wagener, H. Halling, S. Mantl, Nuclear Instruments and Methods B 161–163 (2000) 227.
[36] D. Buca, B. Holländer, S. Feste, H. St. Lenk, S. Trinkaus, R. Mantl, Loo,
M.   Caymax, Applied Physics Letters 90 (2007) 032108.
[37] R.A. Minamisawa, D. Buca, H. Trinkaus, B. Holländer, S. Mantl, V. Destefanis, J.M. Hartmann, Applied Physics Letters 95 (2009) 034102.
[38] B. Holländer, S. Mantl, B. Stritzker, H. Jorke, E. Kasper, Journal of Materials Research 4 (1989) 163.
[39] T.S. Perova, J. Wasyluk, K. Lyutovich, E. Kasper, M. Oehme, K. Rode, A. Waldron, Journal of Applied Physics 109 (2011) 033502.
[40] V.R. D'Costa, J. Tolle, R. Roucka, C.D. Poweleit, J. Kouvetakis, J. Menendez, Solid State Communications 144 (2007) 240.
[41] S. Su, W. Wang, B. Cheng, W. Hu, G. Zhang, C. Xue, Y. Zuo, Q. Wang, Solid State Communications 151 (2011) 647.
[42] E. Kasper, M. Kittler, M. Oehme, T. Arguirov, Photonics Research 1 (2013) 69.
[43] J. Menendez, H. Hochst, Thin Solid Films 111 (1984) 375.
[44] R. Schorer, W. Wegscheider, G. Abstreiter, Journal of Vacuum Science and Technology B 11 (1993) 1069.